Modular Phenomenological Model for Vented Explosions and its Validation with Experimental and Computational Results

Anubhav Sinha, Vendra C. Madhav Rao, Jennifer X. Wen*
School of Engineering, University of Warwick,
Coventry CV4 7AL, UK
**Corresponding author: Jennifer.Wen@warwick.ac.uk*

Abstract – *The present study reports a modular engineering model for predicting peak pressure in vented explosions. Modelling assumptions are explained in detail and model components are validated against experimental and computational results. A basic version of this model is reported in our earlier paper (Sinha et al. [1]). Previous experimental and modelling efforts on vented explosion have primarily focussed on idealized condition of empty container with uniformly mixed fuel. However, in real accidents, there are often obstacles in flame path, and a leaked fuel may not get enough time to mix uniformly. These realistic accidental scenarios are accounted for in this extended model. The model is further simplified, and a final equation is proposed which depend on two fuel related parameters and two geometric parameters. Fuel parameters are pre-tabulated, and geometric parameters are easy to compute. Procedure to compute pressure generated by external explosion and internal pressure are outlined in detail. Experimental results available in open literature are used to evaluate model prediction capabilities. The model, in principle should be applicable for any gaseous fuel. However, the focus of the present investigation is to assess it for hydrogen explosions.*

In parallel to the modelling effort, a dedicated in-house solver HyFOAM is developed utilizing OpenFOAM platform. The HyFOAM predictions are validated against experimental results from the recently published test data involving hydrogen explosion in a 20-feet ISO container (Skjold et al. [2-4]). Moreover, as experimental investigations are expensive and require significant testing and safety infrastructure, a limited number of scenarios can be tested experimentally. In

addition to the experimental results, few more cases are simulated using HyFOAM and engineering model results are compared with the CFD results, and a reasonably good match is observed.

1. Introduction

Explosion venting of low strength enclosures and buildings is one of the most common methods to relive pressure. It has been employed in various industrial and safety installations as a method to mitigate the risk of building damage during accidental explosions. Calculation of overpressure generated for various conditions is an important parameter in vent design. There have been several investigations on vented explosions using gaseous hydrocarbon like methane, propane [5-6], vapour formed by spillage of liquid hydrocarbons and dust explosions [7-11]. Hydrogen, which has a higher flame speed than hydrocarbons and prone to flame instabilities [12] which make it potentially more damaging, has scarcely been studied as extensively as other fuels. Hydrogen explosions are relevant to nuclear power plants operating with water in contact with metal (Zirconium) components at elevated temperatures and pressures. As water corrodes these metal components, hydrogen is formed, accumulated, and if not treated properly, may result in explosion. Fukushima accident in 2011 was the result of explosion of hydrogen accumulated this way [13]. Hydrogen safety is also highly relevant to the chemical and process industries [14]. It finds application in fuel cells, rocket propulsion, metallic ore reduction, oil and fat hydrogenation, etc. Several important chemicals like ammonia, methanol, fertilizers, etc. require hydrogen for their production. Hydrogen has also been recognized as a potential clean energy carrier in past few years. This increased interest in hydrogen calls for a comprehensive investigation in hydrogen safety, recognizing potential hazards, and methods to mitigate them. This paper focuses on hydrogen deflagration and its pressure relief through vent panels.

Engineering models provide a fast and efficient way for pressure prediction in vented explosions. A comprehensively validated model will be very useful for safety assessment of industrial or domestic installations having the risk of accidental explosions. A major challenge with available models is that most of them are based on empirical correlations of experimental results rather than physical reasoning. Due to their empirical nature, the model framework also becomes rigid

and not modular. A modular model will be helpful in incorporating any new conditions by adding sub-models to account for them. It will also be easier to assess each sub-model or constituent framework of the model against experimental data. The performance of these models and their limitations for practical conditions are highlighted in our recent reviews [1, 15, 16]. Moreover, model validation effort with experiments is also limited, especially for hydrogen explosions. This can be attributed to fewer experimental studies being available, especially for hydrogen, and at realistic conditions. To address this issue, a large number of tests are conducted with hydrogen at realistic conditions in a 20-foot ISO container (Skjold et al. [2 -4]). Additionally, computational efforts are also focused on developing an in-house code that can simulate explosion phenomenon accurately. A dedicated in-house solver HyFOAM based on OpenFOAM platform is developed and validated against experimental data from [2-4]. This validated code can further be used to validate engineering models. The present study focusses on defining and validating an engineering model with available experimental and computational results. The effort is to maintain the model framework modular; and add sub-models to account for realistic accidental scenarios.

2. Physical Processes involved in Venting

The model considers the physical processes involved in vented explosion. The advantage is that all processes are considered separately in a modular fashion. Some correlations, like the flame propagation velocity are based on experimental observation and can be improved when more accurate measurements are available, without altering the basic framework of the model. The processes considered in this model are:

2.1. Internal Flame Propagation

2.2. Unburnt gas Venting and External Cloud Formation

2.3. External Explosion

2.4. Internal Pressure Rise

All these processes will be discussed in the following sections and modelling assumptions will be validated with experimental and computational results

2.1. Internal flame propagation

The most critical parameter which affects the internal overpressure is the internal flame propagation. The flame propagation from source of ignition to the vent is a complex phenomenon which is challenging to model. However, flame propagation can broadly be attributed to a combination of two processes – spherical flame propagation, and bulk gas motion induced by venting. These processes are shown schematically in Fig. 1.

(a) Spherical flame propagation

After ignition, the flame propagates outwards into unburnt mixture. Expanding burnt gases also aid in outward propagation of flame-front. This can be modelled using experimental results from Bauwens et al. [17] on spherical flame propagation. The flame velocity in a medium at rest can be described by using the correlation formed by data-fit on Bauwens and co-workers' experimental result.

$$\frac{U_f}{U_0} = \left(\frac{R}{R_0}\right)^{\beta} \tag{1}$$

Where U_f is the flame velocity at radius R, U_0 and R_0 are critical velocity at critical radius, respectively, β is fractal excess. This fractal excess remains constant (β =0.243) for all hydrogen concentrations [17].

(b) Bulk gas motion induced by venting

As pressure rises inside the enclosure, vent opens, and unburnt gases escape out. Venting induces a bulk gas motion towards the vent. This bulk gas motion is also responsible to move the flame towards the vent. This can be modelled using Bernoulli's equation across the vent. Considering two points in the unburnt gases, just inside and outside the vent:

$$\frac{P_1}{\rho_u} + \frac{U_1^2}{2} = \frac{P_2}{\rho_u} + \frac{U_2^2}{2} \tag{2}$$

(a) Spherical Flame Propagation (b) Bulk gas motion induced by venting

Figure 1. Processes contributing to the internal flame propagation.

where subscript 1 is for the internal point and 2 is for the point outside the vent. P_1 denote the internal pressure and P_2 is for the external ambient pressure, U_1 and U_2 are velocities and ρ_u is the unburnt gas density. U_1 is the bulk velocity induced inside the enclosure due to venting. Also, the velocities can be related to each other using equation of continuity and assuming density changes to be negligible. Hence,

$$A_1 U_1 = A_2 U_2 \tag{3}$$

Which can be expressed in terms of enclosure dimensions as:

$$B.H.U_1 = A_v\, U_2 \tag{4}$$

Where B and H are the enclosure breadth and height, respectively, and A_v is the vent area. Eliminating U_2 from equations (2) to (4):

$$U_1 = \sqrt{\frac{2\,\Delta P}{\rho_u \left[\left(\frac{B.H}{A_v}\right)^2 - 1\right]}} \tag{5}$$

Where ΔP denotes overpressure inside the enclosure. Hence, U_1 can be computed for a given overpressure value and enclosure dimensions. Similarly, the variation of U_1 with time can be computed using overpressure variation with time.

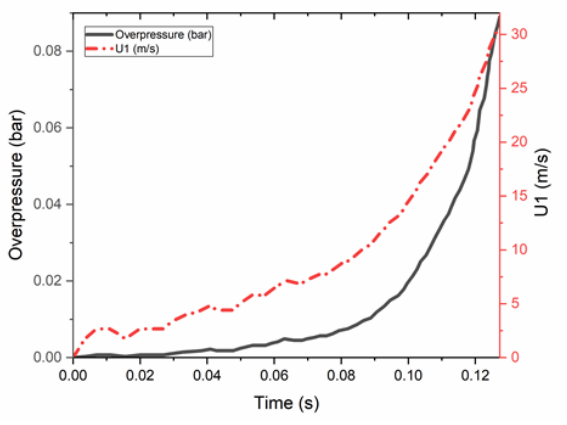

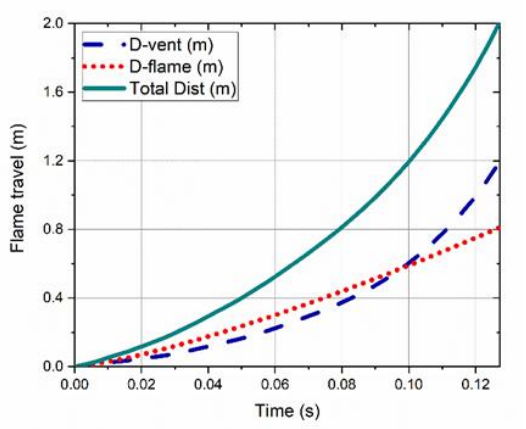

(i) (ii)

(a) H2 – 16.5%

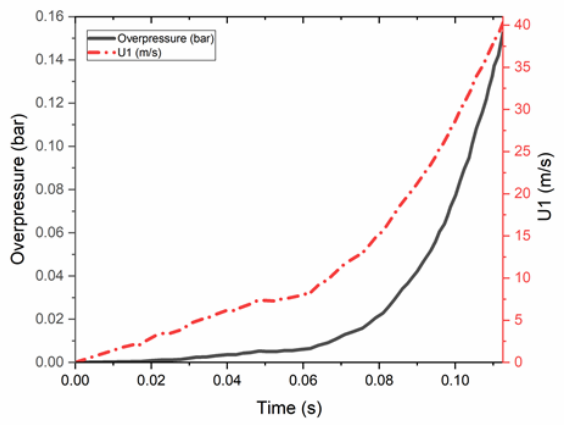

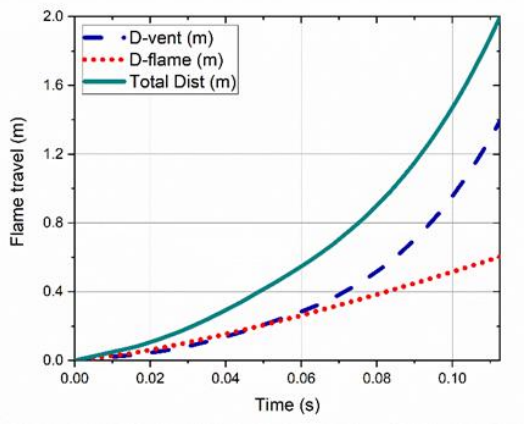

(i) (ii)

(b) H2 – 16 %

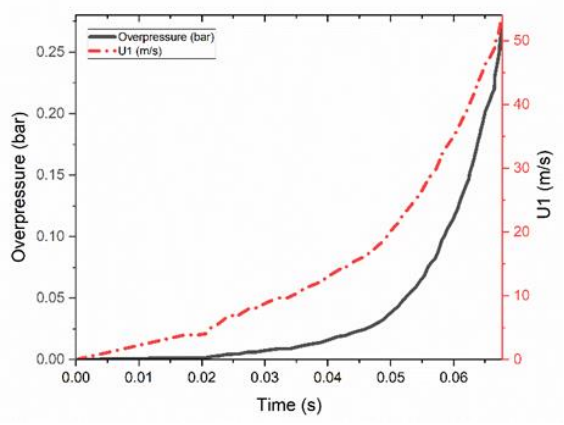

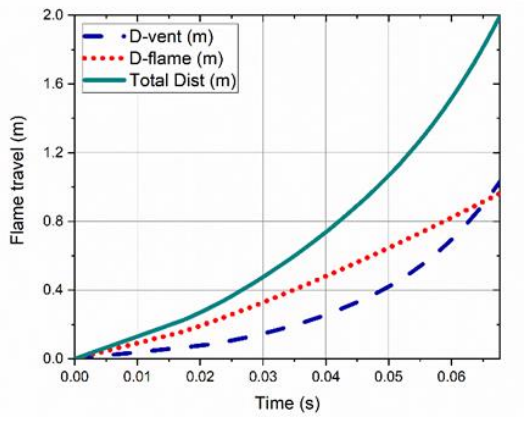

(i) *(ii)*

(c) H2 – 21 %

Fig. 2. (i) Measured overpressure and computed internal velocity (U1) profiles, and (ii) distance travelled by flame showing the contribution of both spherical propagation and vending induced motion; for different fuel concentrations from experiments of [18, 19].

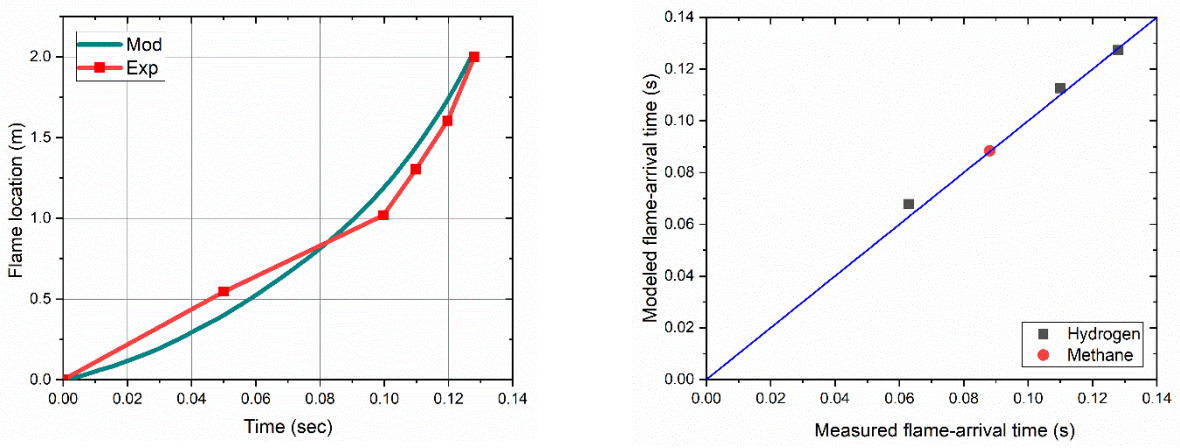

(a) (b)

Fig. 3. Evolution of flame propagation (a) Flame motion away from source of ignition, and (b) Comparison of modeled and experimentally observed flame-arrival time at the vent.

2.1.1. Validation with experimental measurements

As described in the above paragraphs, flame motion inside the enclosure can be attributed to spherical flame propagation and induced bulk velocity due to venting. A mathematical model combing these two effects can be used to estimate the flame position with time. First, the induced velocity variation with time is computed from an overpressure profile using Eq. (5). Further, the flame motion due to spherical flame propagation can be calculated using Eq. (1). Using both the velocities, distance travelled by flame with time can be computed.

Fig. 2 shows calculation for flame travel using the above model for experiments of Daubech et al. [18, 19]. First induced velocity (U_1) profile is computed using experimentally measured pressure profile. This is shown in the left column of Fig. 2. As vent opening time is not available, it is assumed that the vent opens shortly after ignition. Further, distance travelled by flame due to induced velocity and spherical propagation are separately computed and shown in the plot in the right column of Fig. 2. *D-vent* denotes the flame motion induced by bulk gas motion due to venting, and *D-flame* denotes the flame motion due to spherical propagation. Total distance travelled by flame is plotted as a sum of these two components. Calculations are carried out till the flame reaches the vent which is 2 m away from the ignition point for this enclosure [18]. Results are shown for different hydrogen concentrations. It is interesting to note that there is a significant difference in cases shown in (a) and (b) while the hydrogen concentrations differ only by 0.5%. This highlight the issue of repeatability of experiments and a challenge for modelling efforts. Another noteworthy point is the relative contribution from spherical propagation (*D-flame* in Fig. 2) and venting induced motion (*D-vent* in Fig. 2). For lower fuel concentrations (Fig. 2(a) and 2(b)), the contribution from venting inducted motion is dominant, whereas for higher fuel concentration (where flame speed is higher), the contribution from spherical flame propagation and venting induced motion is comparable. It is also to be noted that experiments in

[19] also include initial turbulent cases. Only cases with quiescent mixture is considered in the present study.

Experimentally measured flame-front location, and time required for flame to reach the vent are important parameters to assess the applicability of the present model. Daubech et al. [18-20] have measured time required for the flame to reach the vent, and the flame-front position with time (for case with 16.5% hydrogen) [18, 21]. Comparison flame-front motion computed using this model and measured values are presented in Fig. 3(a). Moreover, measured and computed times for flame to reach vent is also shown in Fig. 3(b). In addition to the hydrogen tests, one test with methane carried out at the same facility (Proust and Leprette [22]) is also included. As evident, the measurements and model results show a very good match, further validating the present modelling approach. Please note that these are the only available experimental investigations in literature where flame arrival time (FAT) is reported.

(a) HySEA Experiments with 20-feet ISO Containers

Further, there is a large set of experimental results of vented hydrogen explosion in a 20-foot ISO container under the aegis of HySEA project (Skjold et al. [2-4]). Overpressure measurements are reported for these experiments. High-speed images are also captured which can be used to estimate vent opening times and flame arrival time to the vent. For these experiments it was also possible to extract the vent opening time (*Tv*). Venting process starts after *Tv* and hence induced velocity (U_1) is zero before this time. The time instance *Tv* is marked in these plots for clarity. Case numbers assigned in the report [3] are retained to avoid confusion, and ease of cross referencing.

(i) Effect of Vent Area

Computations carried out for HySEA experiments are shown in Fig. 4. All cases shown in Fig. 4 are conducted with hydrogen concentration of 21% and empty enclosure with roof vented configurations. In these experiments vent is covered with plastic sheet. Fig. 4 shows the effect of variation of vent area. Velocity plots show an increase in internal velocity with increasing vent area. This could be attributed to higher venting for larger vent area resulting in a larger induced velocity. It is also noteworthy that the vent opening time and flame arrival time are not much different between these three cases. However, there is a slight increase in *Tv* with increasing vent area. Another relevant parameter under consideration is the relative contribution from spherical propagation (*D-flame*) and venting induced motion (*D-vent*). It is observed that spherical propagation is the dominant mode for smaller vent area (see Fig. 4(a)(ii)), while the contribution from venting induced motion increases with vent area and becomes comparable to spherical propagation at the largest venting area (see Fig. 4(c)(ii)). This can also be attributed to the increase in gas venting with increasing vent area.

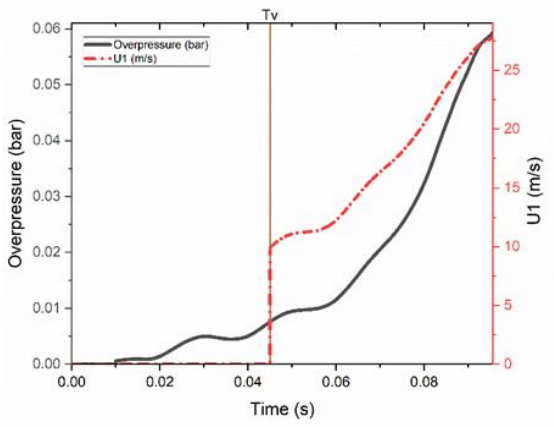

(i)

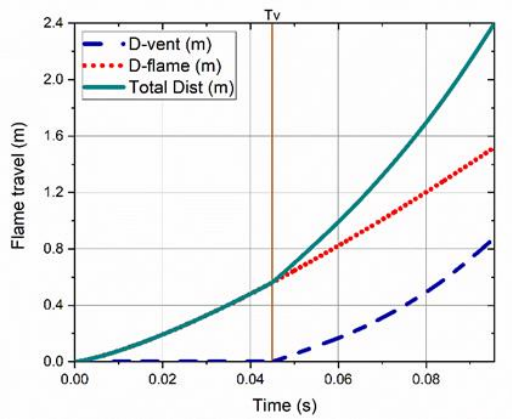

(ii)

(a) Case 25 – Av = 4 m^2

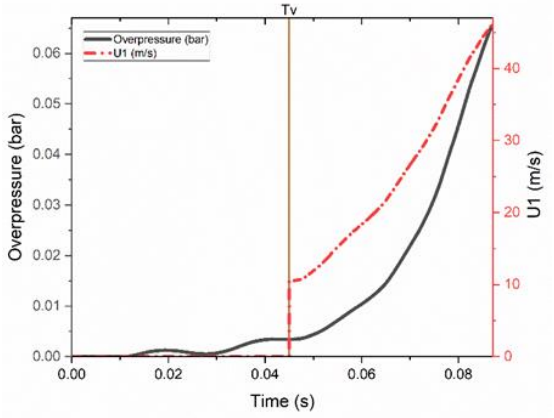

(i)

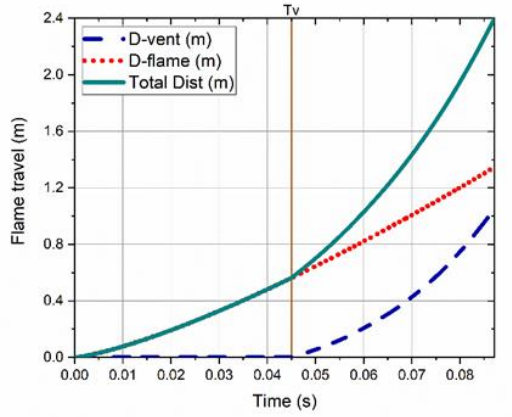

(ii)

(a) Case 21 – Av = 6 m^2

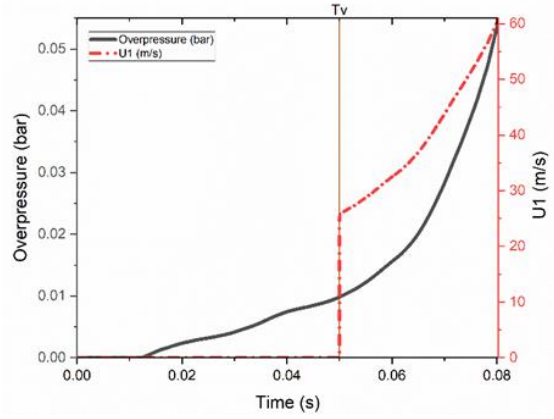

(i)

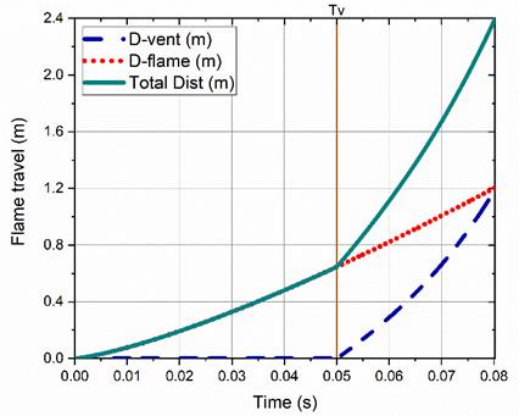

(ii)

(c) Case 16 – Av = 8 m^2

Fig. 4. (i) Measured overpressure and computed internal velocity (U1) profiles, and (ii) distance travelled by flame showing the contribution of both spherical propagation and vending induced motion; for different vent area from HySEA experiments [2-4].

(ii) Effect of Vent Cover

The HySEA experiments are conducted using two set of vent covers. The vents are covered either with plastic sheets or with commercial vent panels. A comparison of flame travel for both conditions is shown in Fig. 5. Case 25 has been investigated using plastic covers and commercial vent panels have been tested in Case 32. They have the same hydrogen concentration (21%) and vent area (Av=4 m^2). Vent opening times and peak pressures are higher for cases with commercial vent panel. Due to delayed vent opening, the flame travels predominantly due to spherical expansion. Hence, the relative flame speed with respect to the unburnt mixture is higher in tests with commercial vent panels, which is responsible for higher peak pressure. Another topic of interest might be the effect on vent panel opening on external cloud and cloud combustion. However, this is beyond the scope of the present study.

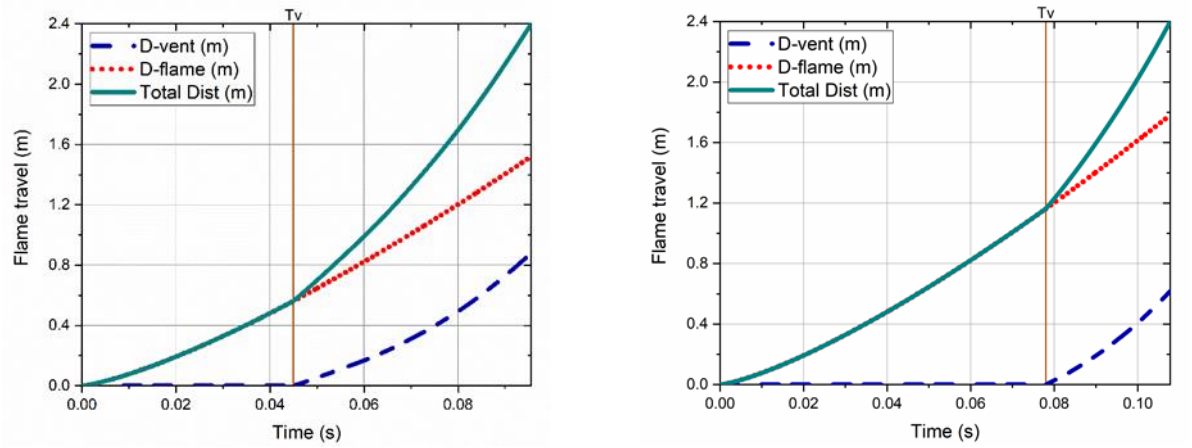

(a) Case 25 – plastic cover (b) Case 32–commercial vent panel

Fig. 5. Effect of vent covers – commercial vent panels and plastic sheets.

(iv) Flame arrival time (FAT) predictions

Applying the equations for flame travel explained in this section (Eq. (1) and (5)), time required for the flame to reach the vent is predicted. These predictions are then compared to measured flame arrival time (FAT) in Fig. 6. A reasonable match is observed. However, for all cases the FAT is overpredicted by the present theoretical formulation. On the other hand, a very good match is found in similar calculations for the experiments of Daubech et al. [18-20] shown in Fig. 3. This can be explained as follows. As the GexCon cases are in roof-vented configuration, buoyancy will also play a role in accelerating the burnt gases. This will reduce the FAT compared to cases where buoyancy is not important (as in Fig, 3). Since in the present simplified analysis, buoyancy is not accounted for, the FAT predictions are higher than the measured FAT values.

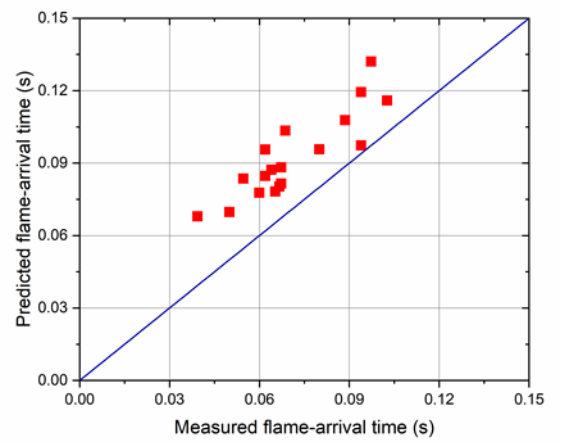

Fig, 6. Comparison of predicted and experimentally measured flame arrival time for HySEA experiments.

2.2. Unburnt gas Venting and External Cloud Formation

Unburnt gas venting and external cloud formation is a complex process which results in external explosion. The vortex roll-up mechanism is clearly observed in experimental [18] and computational investigations [23] as shown in Fig. 7.

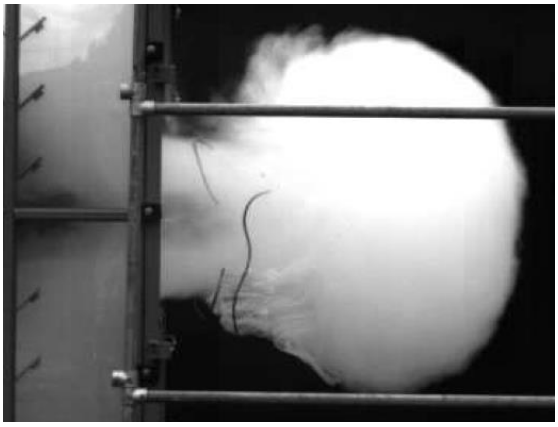

(a) Cloud formation visualized experimentally [18]

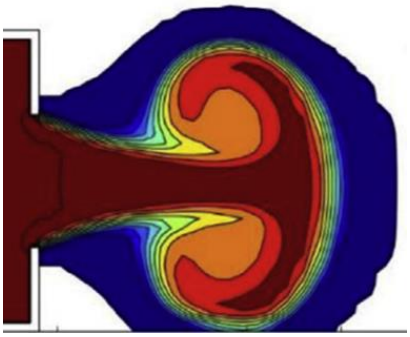

(b) Cloud formation by vortex-roll up as shown in CFD studies of [23]

Fig. 7. Cloud formation by vented gases – (a) Experimental visualization, and (b) CFD simulation.

This behavior can be accounted for using a detailed analysis presented in our previous work (Sinha and Wen [24]). However, the detailed procedure is quite tedious and not suitable for a simplified model. Further, it was observed that the cloud dimensions primarily depend on the enclosure volume. Average radius values from detailed analysis considering enclosure

geometries from reported experiments with hydrogen [7, 18, 25, 26] are shown in Fig. 8(a). It seems the calculated values can be conservatively approximated by a curve fit:

$$R_{Cl} = 0.5\, V^{\,0.3} \tag{6}$$

where R_{Cl} is the external cloud radius and V is the enclosure volume. The curve-fit in Eq. (6) is further tested against experimentally measured cloud radius from Proust and Leprette [22], and Daubech et al. [18] as shown in Fig. 8(b). As evident, predictions from Eq. (6) show a good match with the measured radius values, as well as calculations from the detailed analysis. Please note that the measured radius values shown in Fig. 8(b) are the only experimentally measured cloud dimensions available in literature.

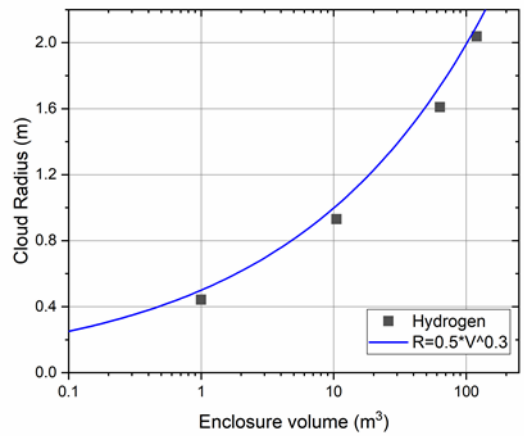

(a) Calculated cloud radius with conservative curve-fit (Eq. (6))

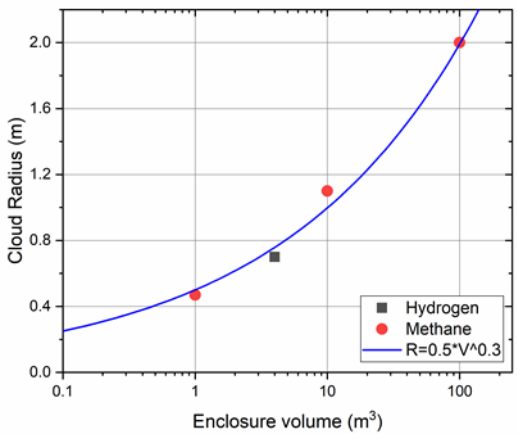

(b) Measured cloud radius compared with curve from Eq. (6).

Fig. 8. Calculated and measured cloud radius compared with predictions from Eq. (6)

2.3. External Explosion

The external cloud formed by gas venting is ignited by the flame approaching the vent. This gives rise to external explosion. Pressure generated due to this external explosion can be modelled using Taylor's spherical piston theory (Strehlow et al. [27]):

$$P_{ext} = \left[2\,\gamma(\sigma^2 - \sigma)\left(\frac{U_{Rcl}}{a_0}\right)^2\right] \tag{7}$$

where σ is the expansion ratio, γ is the ratio of specific heats of unburnt gases, U_{Rcl} is the flame speed at cloud radius (R_{Cl}), and a_0 is the acoustic velocity in unburnt gases. Predictions for overpressure in external explosions are compared with experimentally measured values in the HySEA experiments [3] in Fig. 9. Two configurations are considered – door-vented and roof-

vented. As observed, the predictions show a constant value for external pressure for same fuel concentration. This can be attributed to the fact that Eq. (7) depends only on fuel properties once the cloud radius is known. Overall a good agreement is observed with mostly conservative estimates.

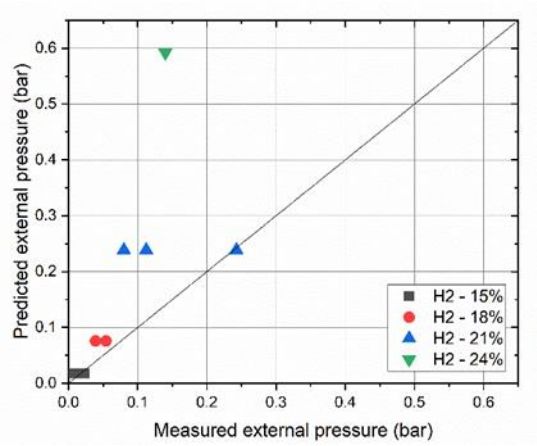

(i) door-vented cases

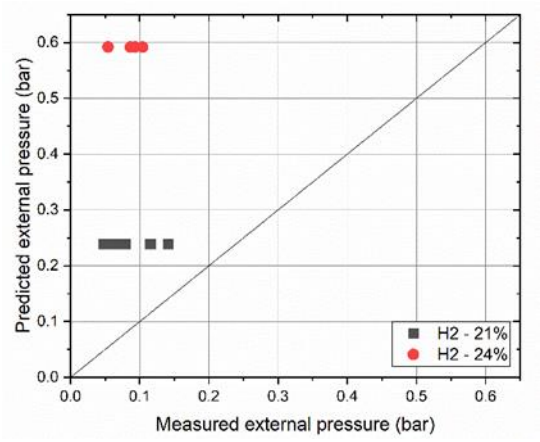

(ii) roof- vented cases

Fig. 9. Comparison of predicted and measured overpressure values in external explosions

2.4. Internal Pressure Rise

The internal pressure maximum is attributed to the peak generated due to external explosion. This can be explained as follows. The internal flame continuously generates burnt gases at high temperature and higher specific volumes. This contributes towards increasing of internal pressure. Venting of unburnt gases keeps a check over internal pressure rise. However, pressure generated from external explosion, partly obstructs the venting process. Hence, the internal pressure builds up and a peak is observed. Gases escaping through the vent due to the pressure difference across the vent can be approximated using a simplified analysis using Bernoulli's equation. Considering two points just inside and just outside the vent while the flame is about to reach the vent

$$\frac{P_1}{\rho_u} + \frac{U_1^2}{2} = \frac{P_2}{\rho_u} + \frac{U_2^2}{2} \tag{8}$$

Where subscript 1 is for the internal and 2 is for the external location. Now, the velocity U_1 can be approximated as:

$$U_1 = U_{Leff}\left(\frac{\sigma - 1}{\sigma}\right) \tag{9}$$

where is U_{Leff} is the flame-speed near the vent computed using Equation 1, σ is the expansion ratio for fuel, and U_{Leff} is the distance between the ignition and vent. Similarly, U_2 can be expressed as:

$$U_2 = \left(\frac{A_f}{A_v}\right) U_{Leff} \left(\frac{\sigma - 1}{\sigma}\right) \tag{10}$$

Where A_f is the flame surface area, and A_v is the vent area. Combining these equations,

$$P_1 - P_2 = \left[\frac{\rho_u}{2}\left\{U_{Leff}\left(\frac{\sigma - 1}{\sigma}\right)\right\}^2 \left\{\left(\frac{A_f}{A_v}\right)^2 - 1\right\}\right] \tag{11}$$

This gives the pressure drop across the vent for the instance when the flame is approaching the vent. It is assumed that approximately the same pressure-drop is maintained at the time of peak pressure. Substituting P_2 with P_{ext} and P_1 with P

$$P = \left[\frac{\rho_u}{2}\left\{U_{Leff}\left(\frac{\sigma - 1}{\sigma}\right)\right\}^2 \left\{\left(\frac{A_f}{A_v}\right)^2 - 1\right\}\right] + P_{ext} \tag{12}$$

Hence, peak internal pressure (P) can be computed using Eq. (12) once the external pressure is known. Please note that in this formulation it is assumed that the induced velocity due to venting process is negligible. This assumption makes this computation simpler and also aids in formulating a conservative model. Another advantage of this assumption is that pressure profile measurements are not required as was needed for computations in section 2.1.

An important parameter in using Eq. (12) or computing peak pressure is the surface area of internal flame (A_f). Daubech et al. [18] and Copper et al. [27] have experimentally visualized flame shape images as shown in Fig. 10. As evident, flame from back-wall ignition can be approximated as a semi-ellipsoid and flame from central ignition case can be approximated as an elongated sphere.

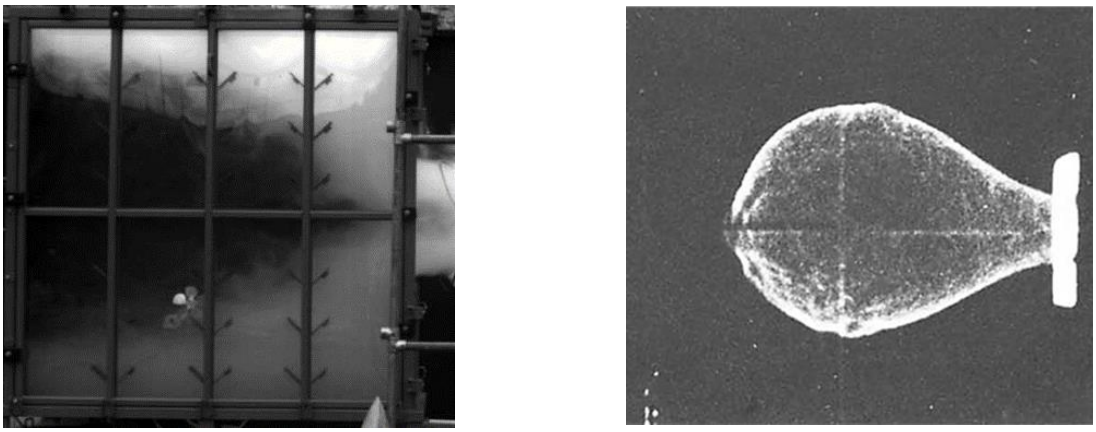

(a) Back-wall ignition case from [18] (b) Central ignition case from [27]

Fig. 10. Flame shape visualizations from [18] and [27]

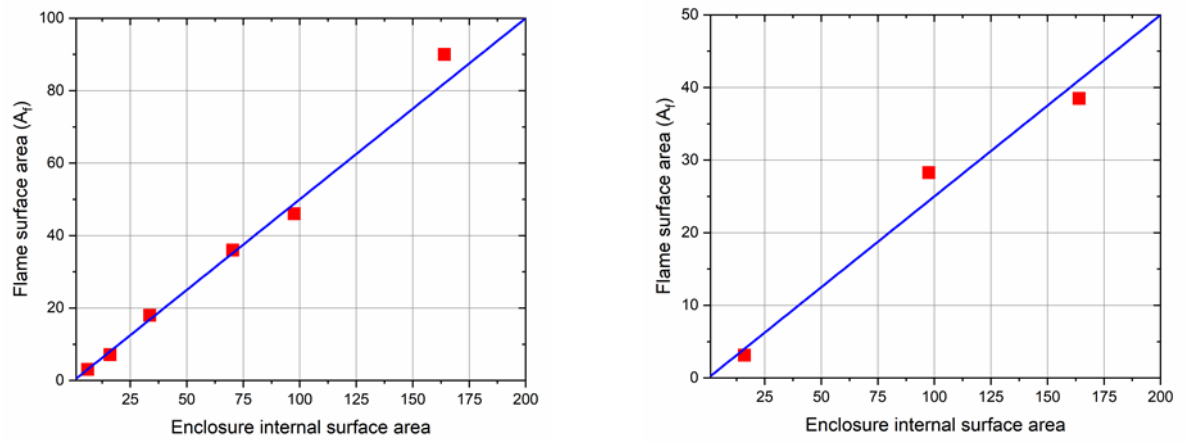

(a) Back-wall ignition (b) Central ignition

Fig. 11. Comparison of enclosure internal surface area with computed values of flame surface areas for different ignition locations.

Assuming these geometric shapes, flame areas for various enclosure geometries (from experiments of [2, 7, 18, 19, 25]) are computed. A comparison of computed flame areas with enclosure internal surface areas is shown in Fig. 11. It is observed that the flame surface area (A_f) can be estimated as a fraction of enclosure surface area (A_{in}).

$$A_f(BWI) = 0.5\, A_{in} \tag{13}$$

$$A_f(CI) = 0.25\, A_{in} \tag{14}$$

for back-wall and central ignition cases respectively. This leads to a significant simplification for the final model equations. Eq. (13) and (14) can be also combined in a same equation using a multiplying factor *x*:

$$A_f = 0.5\, x\, A_{in} \tag{15}$$

where

$$x = \begin{cases} 1 & \text{for Back} - \text{wall ignition (BWI)} \\ 1/2 & \text{for central} - \text{ignition (CI)} \end{cases} \tag{16}$$

This factor *x* can also be used to define the distance between the ignition point and vent area (L_{eff}) as:

$$L_{eff} = x\, L \tag{17}$$

Where *L* is the enclosure length.

3. Model Formulation and Simplification

An accurate model for predicting internal overpressure needs to incorporate physical processes listed in section 2. Accounting each process in a sub-component of the model will facilitate to formulate a modular model. This modularity is especially important for future development. As more accurate measurements are made available, model components can be updated while retaining the same basic framework. Moreover, any additional condition not considered in the present development can later be easily appended to the existing model. The model also needs to be sufficiently simple to use to be recommended for standards and safety norms, which is the major objective of this project. Considering the formulations presented to approximate the physical processes in the last section, pressure drop across the vent:

$$P - P_{ext} = \Delta P = \left[\frac{\rho_u}{2}\left\{U_{Leff}\left(\frac{\sigma-1}{\sigma}\right)\right\}^2\left\{\left(\frac{A_f}{A_v}\right)^2 - 1\right\}\right] \tag{18}$$

Where the external pressure (P_{ext}) can be computed from Eq. (7):

$$P_{ext} = \left[2\,\gamma(\sigma^2-\sigma)\left(\frac{U_{Rcl}}{a_0}\right)^2\right] \tag{7}$$

From Eq. (1) and (18):

$$\Delta P = \left[\frac{\rho_u}{2\cdot 10^5}\left\{\frac{U_0}{R_0^\beta}\left(\frac{\sigma-1}{\sigma}\right)\right\}^2\right]\left[\left(L_{eff}^\beta\right)^2\left\{\left(\frac{A_f}{A_v}\right)^2 - 1\right\}\right] \tag{19}$$

Eq. (18) expresses the pressure in N/m^2. A divisor of 10^5 is included in Eq. (18) to convert to *bar*. Further, using Eq. (13)-(17):

$$\Delta P = \left[\frac{\rho_u}{2\cdot 10^5}\left\{\frac{U_0}{R_0^\beta}\left(\frac{\sigma-1}{\sigma}\right)\right\}^2\right]\left[(xL)^{2\beta}\left\{\left(\frac{xA_{in}}{2\,A_v}\right)^2 - 1\right\}\right] \tag{20}$$

A closer examination of Eq. (20) reveals that the terms in the first bracket are completely dependent on fuel properties and terms in the second bracket are a simple function of enclosure geometry. Hence, Eq. (20) can be reduced to:

$$\Delta P = F1\cdot G1 \tag{21}$$

where

$$F1 = \left[\frac{\rho_u}{2\cdot 10^5}\left\{\frac{U_0}{R_0^\beta}\left(\frac{\sigma-1}{\sigma}\right)\right\}^2\right], \tag{22}$$

and

$$G1 = \left[(xL)^{2\beta}\left\{\left(\frac{xA_{in}}{2\,A_v}\right)^2 - 1\right\}\right]. \quad (23)$$

where L is the enclosure length, A_v is the vent area, A_{in} is the enclosure surface area, and x is defined in Eq. (16). Similarly, Eq. (7) can be expressed as:

$$P_{ext} = \left[\frac{2\,\gamma_u(\sigma^2-\sigma)}{a_0^2}\left(\frac{U_0}{R_0^\beta}\right)^2\right]\left[R_{Cl}^\beta\right]^2 \quad (24)$$

Using Eq. (6):

$$P_{ext} = \left[\frac{2\,\gamma_u(\sigma^2-\sigma)}{a_0^2}\left(\frac{U_0}{R_0^\beta}\right)^2\right]\left[0.5\,V^{0.3}\right]^{2\beta} \quad (24)$$

Again, the first bracket is a function of fuel properties and second bracket is a simple function of enclosure volume (V). This can be expressed as:

$$P_{ext} = F2 \cdot G2 \quad (25)$$

where

$$F2 = \left[\frac{2\,\gamma_u(\sigma^2-\sigma)}{a_0^2}\left(\frac{U_0}{R_0^\beta}\right)^2\right] \quad (26)$$

and

$$G2 = \left[0.5\,V^{0.3}\right]^{2\beta} \quad (27)$$

Using Eq. (18) – (27), the internal overpressure can be expressed in a simplified form as:

$$\boldsymbol{P} = (\boldsymbol{F1}\cdot\boldsymbol{G1}) + (\boldsymbol{F2}\cdot\boldsymbol{G2}) \quad (28)$$

where

$$F1 = \left[\frac{\rho_u}{2\cdot 10^5}\left\{\frac{U_0}{R_0^\beta}\left(\frac{\sigma-1}{\sigma}\right)\right\}^2\right], \quad (22)$$

$$F2 = \left[\frac{2\,\gamma_u(\sigma^2-\sigma)}{a_0^2}\left(\frac{U_0}{R_0^\beta}\right)^2\right], \quad (26)$$

$$G1 = \left[(xL)^{2\beta}\left\{\left(\frac{xA_{in}}{2\,A_v}\right)^2 - 1\right\}\right], \quad (23)$$

$$G2 = \left[0.5\,V^{0.3}\right]^{2\beta}. \quad (27)$$

These fuel dependent parameters *F1* and *F2* are pre-tabulated and shown in Appendix. This look up table will be used in model calculations.

3.1. Effect of Obstacles

Obstacles in the flame path are a very common configuration in realistic accidents. However, as pointed out in our recent review [1], most available models do not account for them. While the HySEA experiments [2] show that the presence of obstacles increases the overpressure significantly, as compared to an empty enclosure. Hence, it becomes imperative for any realistic model to include their effect. Flame propagating past obstacles behave similarly to a non-

reacting fluid flowing past a bluff body, i.e. the flame wraps around these obstacles and at the time of peak internal pressure, there is also a contribution from this wrapped flame surface. This wrapped flame can clearly be seen in the CFD visualization in the present study shown in Fig. 12. CFD modelling details are presented in section 4.

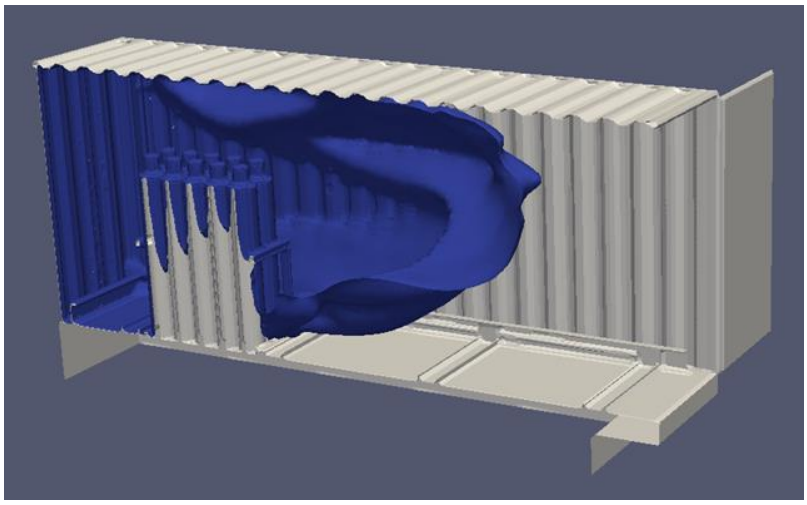

Fig. 12. CFD visualization of flame inside a 20-foot ISO container used for HySEA experiments. A model obstacle used in experiments - bottle basket is shown.

To account for the effect of obstacle, the flame surface area around an obstacle is calculated and added to the flame surface area obtained in Eq. (15). The wrapped flame surface area is calculated as:

$$A_{obs} = (P_{obs} + 1.2\, L_{obs})\; H_{obs} \tag{28}$$

where A_{obs} is the area of wrapped flame around obstacles, P_{obs} is the perimeter of obstacles, H_{obs} is the height of obstacles and L_{obs} is the characteristic length scale of the obstacle. The length of recirculation length is taken as $0.6\, L_{obs}$ utilizing the bluff body simulation from Minguez et al. [33]. This area (A_{obs}) must be added to the flame surface area computed in Eq. (15) for cases having obstacles.

3.2. Effect of Fuel Stratification

Accidental leakage of fuel gases is often the reason behind explosions. Generally, the leaked gases form a stratified mixture and don't get enough time to mix uniformly. This is an important practical configuration which is often overlooked in modelling investigations [1]. The present study aims at developing a model which will be simple to use and also incorporate realistic conditions like stratified mixture. The most critical parameter affecting the internal pressure is believed to be the flame speed. To retain the basic framework of this model and to device a

simple model for stratification, it is decided to use fuel properties of the highest fuel concentration observed and to use the same equations of the basic model. The limitation of this approach is that a measured fuel concentration profile is needed to determine the most reactive layer (highest fuel concentration). Computational models or numerical approaches can also be used to obtain the most reactive layer.

3.3. Comparison of Model Predictions with Experimental Results

The HySEA experiments are undertaken using 20-foot ISO containers. Experiments are conducted in two configurations – door vented, and roof-vented. Two model obstacles are used for these experiments – bottle basket and pipe rack. These configurations are shown in Fig. 13 (a)-13(d). More details about the experimental investigation can be found elsewhere [2-4]. Moreover, to mimic realistic accidental scenarios, it was decided to test a case with stratified mixture and also a case with stratified mixture and obstacle (Pipe rack). These tests are carried out in roof-vented configuration (Skjold et al. [4]). An equivalent fuel concentration of 24% is used for model calculations for the stratified cases. Comparison of predictions from the present model with experimentally measured overpressure values is shown in Fig. 13(e) and 13(f). As evident, a reasonably good match is obtained, with mostly conservative estimates of overpressure. One case which uses both the obstacles in door-vented configuration (P1-B3), overpressure is slightly under-predicted. It appears that the obstacle kept near the vent partially blocked the vent area, hence the observed pressure is higher than the predicted values which included the total vent area. Predictions results are closer to measurements or slightly conservative for all other configurations, including cases with obstacles and stratified mixtures.

It is clear that reasonably good predictions are obtained using the present model. However, it would be desirable to test the model with more results at different conditions. It is also important to understand that experiments are expensive and dangerous to conduct. Several measurement and safety equipment are required for conducting large scale experiments. Also, overhead costs for conducting experiments are also quite high. Hence, it is decided to develop a CFD platform and validate it extensively with experimental results. Once properly validated, it can then be used to generate benchmark results to validate model predictions.

(a) Bottle basket- door vented configuration

(b) Pipe rack- door vented configuration

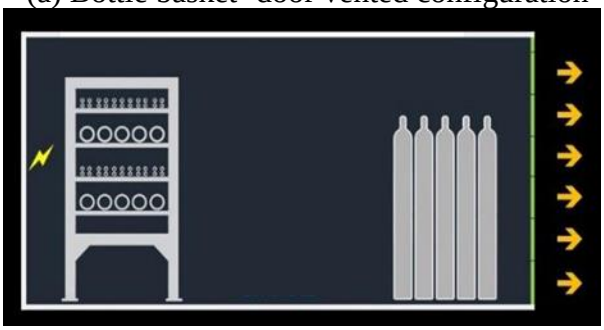

(c) Pipe +Bottle (P1-B3)- door vented configuration

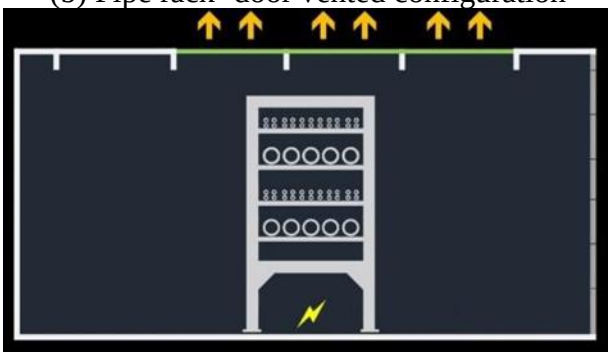

(d) Pipe rack - roof vented configuration

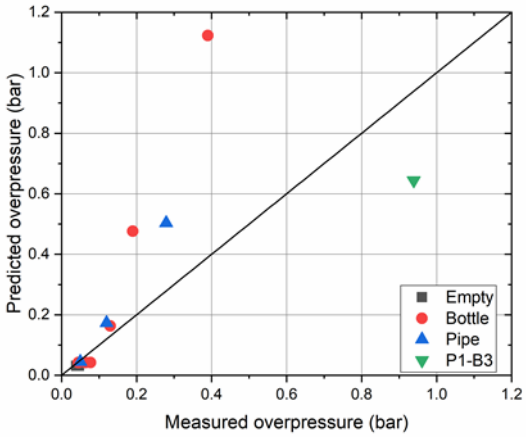

(e) Comparison of predictions and measurement of overpressure for Door vented cases

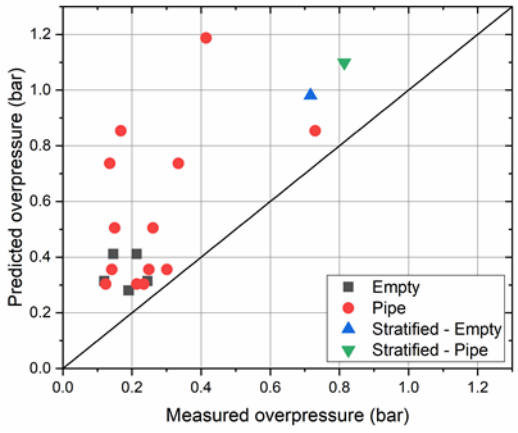

(f) Comparison of predictions and measurement of overpressure for Roof vented cases

Fig. 13. Experimental configurations used and comparison of measured and predicted overpressure for 20-foor container tests.

4. CFD modelling – HyFOAM solver

To model vented explosions of hydrogen, HyFOAM is developed utilizing OpenFOAM platform (OpenFOAM [29]). This code uses fully compressible formulation of the governing equations. Large Eddy Simulations with a one equation eddy viscosity subgrid scale model is used. For modelling combustion, a model proposed by Weller et. al. [30] used. A transport equation for flame regress variable (b), where is b =1-c, (c is the progress variable) is solved. The combustion model source term variables, flame wrinkle factor (Ξ) and the laminar flame speed (S_L) are updated in the solver development with sub-models to account for the Darrieus-Landau, Rayleigh-Taylor instabilities and Lewis effect in lean turbulent flame speed correlation. For low-strength enclosures, such as the ISO containers, enclosure wall deformation also contributes to the pressure rise, and modelling Fluid-structure interaction (FSI) is required to capture the pressure rise accurately. Hence, FSI interaction is also modeled in the present study. The combustion model and the sub-model equations are presented in detail elsewhere [31]. The CFD simulations are performed for the vented lean deflagration in the 20ft ISO container experimental (Skjold et al. [3]) configurations; first to validated against the known experiment test configuration and then carry out the numerical predictions for experimental gap configurations, to aid our understanding of the overall overpressure trends with change in H_2 concentration and model obstacles combinations. Fig. 14 shows the pressure trace curve at the peak overpressure probe location along with experimental measurements at 15% H_2 concentration levels, for container empty and with pipe rack.

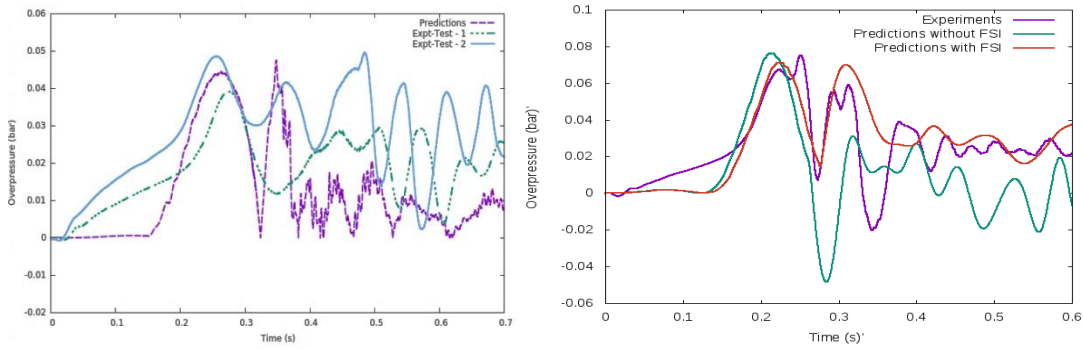

(a) Empty container (b) With bottle basket obstacle

Figure 14. Pressure trace curve at peak overpressure probe location plotted along with experimental measurements for 15% H_2 concentration.

Further, various other cases are simulated, and the peak overpressure is compared with experimental measurements in Table 1. As evident, the CFD model is able to predict experimental values with very god accuracy, even with the cases with obstacles.

Table 1. Comparison of CFD model predictions with experimental overpressure measurements.

H_2%	Configuration	Venting configuration	Vent Area (m2)	P-exp (bar)	P-CFD (bar)
15	Empty	Door vented	5.4	0.042	0.039
15	Bottle (B1)	Door vented	5.4	0.062	0.071
15	Pipe Rack (P1)	Door vented	5.4	0.050	0.063
21	Pipe + Bottle (P1 B3)	Door vented	5.4	0.939	0.938

Further, it is decided to investigate gaps in experimental matrix for fuel concentration and obstacle configuration, which might provide a new data-set to evaluate engineering model prediction. New obstacle configurations to be investigated are shown in Fig. 15. The CFD results and model predictions for the new data sets are shown in Fig. 16. As observed, the model can generate reasonably accurate results for these cases which involve complex obstacle configuration which are challenging to model. The model results are mostly on the conservative side, which is desirable, especially for safety standards requirements. Only two cases are under-predicted. One of them is with P2-B3 configuration where the vent area is partially blocked by the obstacle, as discussed in the previous section.

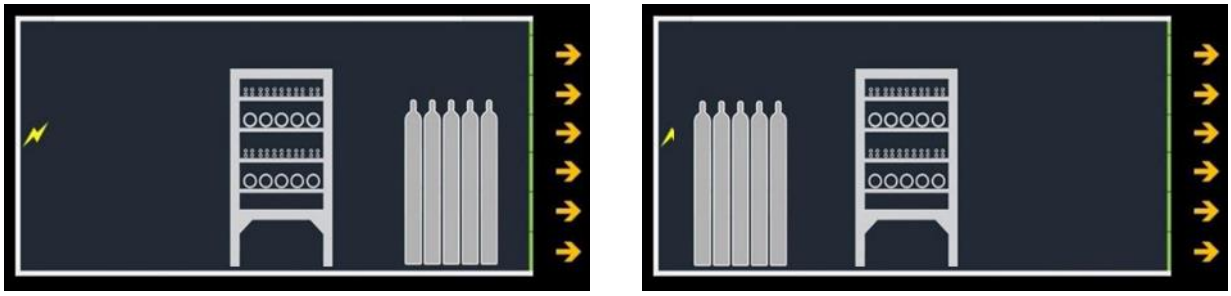

(a) Obstacle configuration – P2-B3 (b) Obstacle configuration – B1-P2

Fig. 15. Various obstacle configuration examined in CFD investigation – door-vented configuration

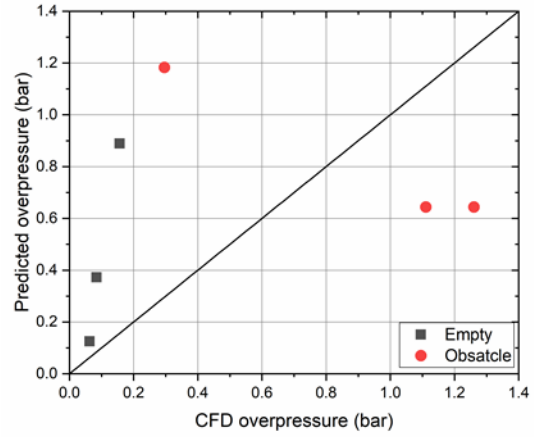

Fig. 16. Comparison of predicted overpressure from the model and CFD results.

5. Conclusions

The present study proposes a modular engineering model to predict overpressure in vented explosions. The model presents various physical processes involved in vented explosions and proposes simplified equations to account for them. The four major processes identified in vented explosions are - Internal flame propagation, Unburnt gas venting and external cloud formation, External explosion, and Internal pressure rise. Experimental measurements available in literature are used to validate various model components. Further, the components are combined to form a simple model with one equation containing four parameters. Two parameters F1 and F2 are fuel dependent and are listed in a table. Geometric parameters G1 and G2 are shown to be simple function of enclosure geometry. The model is validated with the recent HySEA experimental study on 20-foot ISO container. Model predictions are found to be in good agreement with the measured overpressure values. Moreover, a CFD platform based on OpenFOAM is developed and validated with experimental data. CFD platform is further used as generate benchmark results for model validation. Various configurations that were not covered in experiments are modeled using the CFD tool. Model predictions are again compared with CFD results and found to be in good agreement and mostly on the conservative side.

Appendix

H2 %	F1	F2
10	1.7761E-05	1.0417E-03
11	2.3292E-05	1.5248E-03
12	3.5502E-05	2.5724E-03
13	5.7926E-05	4.6089E-03
14	9.5632E-05	8.2934E-03
15	1.5514E-04	1.4562E-02
16	2.4434E-04	2.4661E-02
17	3.7235E-04	4.0159E-02
18	5.4944E-04	6.2953E-02
19	7.8694E-04	9.5249E-02
20	1.0971E-03	1.3953E-01
21	1.4929E-03	1.9849E-01
22	1.9884E-03	2.7497E-01
23	2.5978E-03	3.7187E-01
24	3.3362E-03	4.9201E-01
25	4.2191E-03	6.3805E-01
26	5.2621E-03	8.1227E-01
27	6.4812E-03	1.0165E+00
28	7.8921E-03	1.2520E+00
29	9.5108E-03	1.5189E+00
30	1.1353E-02	1.8169E+00

Table A1. F1 and F2 values for various hydrogen concentrations

References

1. Sinha, A., Rao, M.V.C., Wen, J.X., "Performance Evaluation of Empirical Models for Vented Lean Hydrogen Explosions", *International Journal of Hydrogen Energy* (in press)
2. Skjold, T., Hisken, H., Lakshmipathy, S., Atanga, G., van Wingerden, M., Olsen, K.L., Holme, M.N., Turøy, N.M., Mykleby, M. & van Wingerden, K. (2017). Vented hydrogen deflagrations in containers: effect of congestion for homogeneous mixtures. *ICHS-2017*.
3. Skjold, T., Lakshmipathy, S., van Wingerden, M., Hisken, H., Atanga, G., Olsen, K.L., Holme, M.N., Turøy, N.M., Mykleby, M & van Wingerden, K. (2017). Experimental investigation of vented hydrogen deflagrations in containers – Phase 1: Homogeneous mixtures. *Report HySEA-D2-04-2017,* July 2017: 304 pp.
4. Skjold, T., Hisken, H., Bernard, L., Mauri, L., Atanga, G, Lakshmipathy, S., Carcassi, M., Schiavetti, M.,, Rao, V.C.M., Sinha, A. Tolias, I.C., Giannissi, S.G., Venetsanos, A.G., Stewart, J.R., Hansen, O.R., Kumar, C., Krumenacker, L., Laviron, F., Jambut, R., and Huser, A., Blind-prediction: estimating the consequences of vented hydrogen deflagrations for inhomogeneous mixtures in 20-ft ISO containers, In: ISHPMIE-2018, Kansas, USA.
5. Bauwens, C. Regis, Jeff Chaffee, and Sergey Dorofeev. Effect of ignition location, vent size, and obstacles on vented explosion overpressures in propane-air mixtures. *Combustion Science and Technology* 182.11-12 (2010): 1915-1932.
6. Thomas, J. Kelly, et al. "Elevated Internal Pressures in Vented Deflagration Tests." *AIChE 40th Annual Loss Prevention Symposium.* Orlando, AIChE. 2006.
7. Bauwens, C. Regis, Jeff Chaffee, and S. B. Dorofeev. "Vented explosion overpressures from combustion of hydrogen and hydrocarbon mixtures." *International Journal of Hydrogen Energy* 36.3 (2011): 2329-2336.
8. Eckhoff, Rolf K. Dust explosions in the process industries: identification, assessment and control of dust hazards. *Elsevier*, 2003.
9. Forcier, Tom, and Robert Zalosh. "External pressures generated by vented gas and dust explosions." *Journal of Loss Prevention in the Process Industries* 13.3-5 (2000): 411-417.
10. Baker, Wilfred E., et al. Explosion hazards and evaluation. Vol. 5. *Elsevier*, 2012.
11. Abbasi, Tasneem, and S. A. Abbasi. "The boiling liquid expanding vapour explosion (BLEVE): Mechanism, consequence assessment, management." *Journal of Hazardous materials* 141.3 (2007): 489-519.
12. Matalon, M. (2007). Intrinsic flame instabilities in premixed and nonpremixed combustion. *Annu. Rev. Fluid Mech.*, *39*, 163-191.
13. Yanez, J., M. Kuznetsov, and A. Souto-Iglesias. "An analysis of the hydrogen explosion in the Fukushima-Daiichi accident." *International Journal of Hydrogen Energy* 40.25 (2015): 8261-8280.
14. Ramachandran, R., & Menon, R. K. (1998). An overview of industrial uses of hydrogen. *International Journal of Hydrogen Energy*, *23*(7), 593-598.
15. Sinha, A., Rao, M.V.C., Wen, J.X., Evaluation of Engineering Models for Vented Lean Hydrogen Deflagrations, *ICDERS 2017*, Boston, 2017.
16. Sinha, A., Rao, V. C. M., & Wen, J. X. (2018). Performance evaluation of empirical models for vented lean hydrogen explosions. *In: ICHS-217*, Hamburg.
17. Bauwens, C. R. L., J. M. Bergthorson, and S. B. Dorofeev., Experimental investigation of spherical-flame acceleration in lean hydrogen-air mixtures. *International Journal of Hydrogen Energy* 42.11 (2017): 7691-7697.

18. Daubech, J., Proust, C., Gentilhomme, O., Jamois, C., & Mathieu, L. (2013, September). Hydrogen-air vented explosions: new experimental data. In: *5th International Conference on Hydrogen Safety, Brussels, Belgium.*
19. Daubech, J., Leprette, E., Duclos, A., & Proust, C. (2018, August). Accounting for turbulence in gas explosion venting design. In 12. *International symposium on hazards, prevention, and mitigation of industrial explosions* (ISHPMIE).
20. Jallais, S., *Private communications*, 2018.
21. Vyazmina, E., Jallais, S., Krumenacker, L., Tripathi, A., Mahon, A., Commanay, J., ... & Rosset, F. (2018). Vented explosion of hydrogen/air mixture: An inter-comparison benchmark exercise. International Journal of Hydrogen Energy.
22. Proust, C., & Leprette, E. (2010). The dynamics of vented gas explosions. *Process Safety Progress*, 29(3), 231-235.
23. Li, J., & Hao, H. (2017). Internal and external pressure prediction of vented gas explosion in large rooms by using analytical and CFD methods, *Journal of Loss Prevention in the Process Industries*, 49, 367-381.
24. Sinha, A., Wen, J.X., Phenomenological Modelling of External Cloud Formation in Vented Explosions, *ISHPMIE-2018*, Kansas, USA, Aug 2018.
25. Kumar, Krishna. "Vented combustion of hydrogen-air mixtures in a large rectangular volume." *44th AIAA Aerospace Sciences Meeting and Exhibit*. 2006
26. Daubech, J., Proust, C., Jamois, D., Leprette, E. (2011, September). Dynamics of vented hydrogen-air deflagrations. In *4. International Conference on Hydrogen Safety* (ICHS 2011)
27. Cooper, M. G., Fairweather, M., & Tite, J. P. (1986). On the mechanisms of pressure generation in vented explosions. *Combustion and flame*, 65(1), 1-14.
28. Minguez, M., Brun, C., Pasquetti, R., & Serre, E. (2011). Experimental and high-order LES analysis of the flow in near-wall region of a square cylinder. *International Journal of Heat and Fluid Flow*, 32(3), 558-566.
29. www.openfoam.org
30. Weller, H. G., Tabor, G., Gosman, A. D., and Fureby, C., (1998), Application of a flame wrinkling LES combustion model to a turbulent mixing layer (1998), Proc. of Combust. Institute.
31. Vendra C. Madhav Rao, Wen, J.X., (2018), Fluid structure interactions modelling in Vented lean deflagrations, 12th International Symposium on Hazards, Prevention, and Mitigation of Industrial Explosions (ISHPMIE), Kansas, USA, Aug 2018.